Available online at www.sciencedirect.com
SCIENCE DIRECT
Geochimica et Cosmochimica Acta 70 (2006) 3549–3565
Geochimica
www.elsevier.com/locate/gca

Cation sorption on the muscovite (0 0 1) surface in chloride solutions using high-resolution X-ray reflectivity

Michel L. Schlegel [a,1], Kathryn. L. Nagy [a,*,2], Paul Fenter [b], Likwan Cheng [b], Neil C. Sturchio [c], Steven D. Jacobsen [a,3]

[a] *Department of Geological Sciences, University of Colorado at Boulder, Boulder, CO 80309, USA*
[b] *Chemistry Division, Argonne National Laboratory, Argonne, IL 60439, USA*
[c] *Department of Earth and Environmental Sciences, University of Illinois at Chicago, Chicago, IL 60607, USA*

Received 17 June 2005; accepted in revised form 14 April 2006

Abstract

The structure and mechanism of cation sorption at the (0 0 1) muscovite-water interface were investigated in 0.01 and 0.5 m KCl, CsCl, and $CaCl_2$ and 0.01 m $BaCl_2$ solutions at slightly acidic pH by high-resolution X-ray reflectivity. Structural relaxations of atom positions in the $2M_1$ muscovite were small ($\leqslant$0.07 Å) and occurred over a distance of 30 to 40 Å perpendicular to the interface. Cations in all solutions were sorbed dominantly in the first and second solution layers adjacent to the mineral surface. The derived heights of the first solution layer in KCl and CsCl solutions, 1.67(6)–1.77(7) and 2.15(9)–2.16(2) Å, respectively, differ in magnitude by the approximate difference in crystallographic radii between K and Cs, and correspond closely to the interlayer cation positions in bulk K- and Cs-mica structures. The first solution layer heights in $CaCl_2$ and $BaCl_2$ solutions, 2.46(5)–2.56(11) and 2.02(5) Å, respectively, differ in a sense opposite to that expected based on crystallographic or hydrated radii of the divalent cations. The derived ion heights in all solutions imply that there is no intercalated water layer between the first solution layer and the muscovite surface. Molecular compositions were assigned to the first two solution layers in the electron density profiles using models that constrain the number density of sorbed cations, water molecules, and anions by considering the permanent negative charge of the muscovite and average solution density. The models result in partial charge balance (at least 50%) by cations sorbed in the first two layers in the 0.01 m solutions and approximately full charge balance in the 0.5 m solutions. Damped oscillations of model water density away from the first two solution layers agree with previous X-ray reflectivity results on the muscovite (0 0 1) surface in pure water.

1. Introduction

The basal surface of layered silicates such as micas and clays usually carries a permanent negative charge arising from structural heteroionic substitutions. This charge is balanced by the sorption of both inorganic and organic cationic species (Bolt, 1979; Sposito, 1984; Laudelout, 1987; McBride, 1994) and/or the association of a diffuse layer of ions extending into solution. Sorption and ion-exchange on layered silicates affects the mobility of major and trace elements in soils and sediments, which in turn controls the bioavailability of micronutrients and the transport of toxic or radioactive pollutants. Macroscopic and microscopic experimental results indicate that certain anions may cosorb with cations on mica basal surfaces (Griffoen and Appelo, 1993; Xu and Salmeron, 1998; Maurice and Namjesnik-Dejanovic, 1999; Gier and Johns, 2000; Namjesnik-Dejanovic and Maurice, 2001) and on clay surfaces (Sposito et al., 1981, 1983b; Sposito, 1984, 1991;

* Corresponding author. Fax: +1 312 413 2279.
E-mail address: klnagy@uic.edu (Kathryn. L. Nagy).
[1] Present address: CEA—Saclay, DPC/SCP/LRSI, Bât. 391; F-91191 Gif-sur-Yvette Cedex, France.
[2] Present address: Department of Earth and Environmental Sciences, University of Illinois at Chicago, 845 W. Taylor St., MC-186, Chicago, IL 60607-7059, USA.
[3] Present address: Department of Geological Sciences, Northwestern University, Evanston, IL 60208, USA.

0016-7037/$ - see front matter © 2006 Elsevier Inc. All rights reserved.
doi:10.1016/j.gca.2006.04.011

Karmakar et al., 1991; Chorover and Amistadi, 2001). The energetics of sorption and ion-exchange reactions at the basal surface of micas and clays should depend on both the extent of structural rearrangements at the layered silicate surface (i.e., surface relaxations) and the mechanism of charge compensation, which have yet to be investigated in situ at the molecular-scale.

Direct measurement of atom positions across the layered silicate (0 0 1)-water interface would provide a way to assess the mechanisms of ion sorption without invoking a priori the classical concepts of inner- and outer-sphere sorption (Sposito, 1989) or models based on electrical double layer theory (e.g., Davis and Kent, 1990). X-ray reflectivity measurements using a high-brilliance synchrotron source provide such a detailed atomic-scale description. The X-ray reflectivity, defined as the ratio of the reflected to incident X-ray flux, is measured as a function of the incident angle of the X-ray beam with respect to the surface plane. The weak surface reflectivity observed between bulk Bragg peaks of the substrate crystal is directly related to the electron density profile at the mineral-water interface, and therefore can be used to derive the positions of atoms across this interface (Fenter and Sturchio, 1999; Fenter et al., 2000a; Cheng et al., 2001; Fenter, 2002). Because the measurement requires atomically flat surfaces over an area of a few tenths to a few square millimeters, it cannot be applied to layered clay minerals, for which only micrometer-sized specimens are available. In contrast, muscovite, which has a similar structure to aluminosilicate clays, can be obtained as large single crystals, making it possible to investigate the characteristic interface between a permanently-charged basal siloxane sheet and an aqueous solution. In this paper, we report results of in-situ X-ray reflectivity measurements on muscovite single crystals in chloride electrolyte solutions of monovalent (K^+, Cs^+) and divalent (Ca^{2+}, Ba^{2+}) cations. Models of derived electron density profiles perpendicular to the interface yield new information concerning the number and distribution of ions near the interface, thus providing new insight into ion sorption mechanisms.

2. Background

The platy morphology of layered silicates results from their anisotropic structure (Fig. 1). Muscovite layers are composed of two tetrahedral sheets in which each (Si, Al) tetrahedron shares three basal plane oxygens with neighboring tetrahedra and one apical oxygen with an interposed (Al, Mg, Fe) octahedral sheet. Substitution of Si^{4+} by Al^{3+} results in a net negative charge that is balanced by interlayer K^+ positioned in ditrigonal siloxane cavities, at approximately 1.70 Å above the outermost oxygen atoms of the basal plane. Interlayer K^+ binds layers together via electrostatic forces. Truncation of this structure along the (0 0 1) cleavage direction results in two exposed surfaces, each with a charge of 1 e^- per unit cell surface area (A_{uc}), an area of approximately 47 $Å^2$ that contains two ditrigonal siloxane sites. This negative surface charge must be balanced by direct adsorption of cations or through association of ions to the surface in a "diffuse layer" profile. Adsorbed cations may be located either directly above (or within) the ditrigonal siloxane cavity, or above the basal plane of oxygens (Boek et al., 1995; Skipper et al., 1995). In deionized water, the negative charge per A_{uc} is compensated presumably with a hydronium ion, which is indistinguishable from a water molecule as measured by X-ray scattering, and is likely located within one siloxane cavity or above the tetrahedral basal-plane site (Cheng et al., 2001).

Sorbed cations generally are considered to either retain their hydration water, forming outer-sphere (OS) surface complexes, or dehydrate at least partially and coordinate to oxygens of the silicate mineral surface, forming inner-sphere (IS) surface complexes (Sposito, 1989). Whether or not a cation sorbs as an inner- or outer-sphere complex on phyllosilicate basal planes can be related to the hydra-

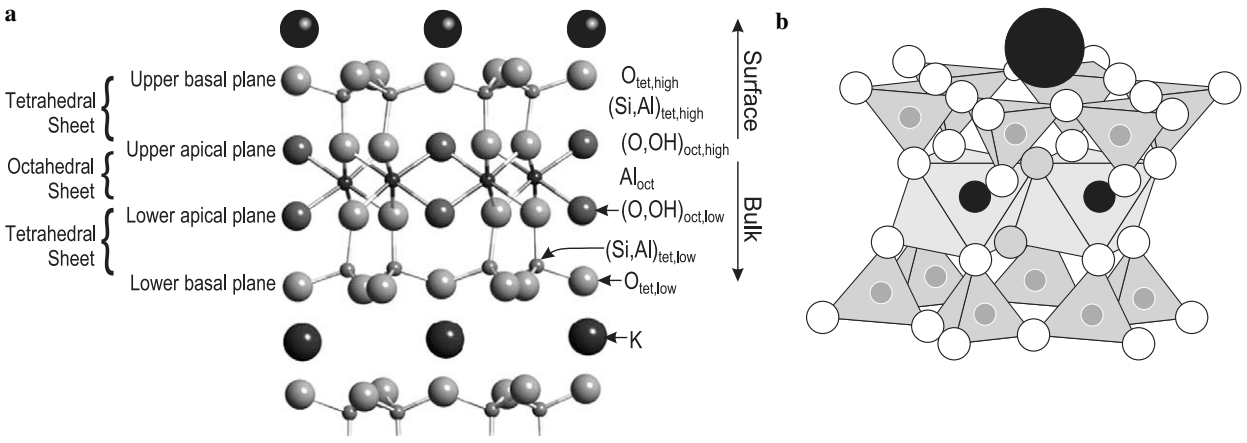

Fig. 1. (a) Crystal structure of muscovite viewed normal to the (1 0 0) plane. Each layer contains an Al octahedral sheet sandwiched by two (Si, Al) tetrahedral sheets. Substitution of Si^{4+} by Al^{3+} in the tetrahedral sheets gives the layers a permanent negative charge that is balanced by interlayer K^+ cations located in ditrigonal cavities on the basal plane. (b) Tilted polyhedral view of a layer showing the location of interlayer K^+ in ditrigonal cavities.

tion energy of the cation in solution: the more negative the hydration energy, the more stable the cation–water association, and the more outer-sphere the sorbed complex (Bérend et al., 1995; Cases et al., 1997). Bond angles and bond lengths between atoms at and near the muscovite surface will adjust to minimize the interfacial energy generated by cleaving and this atomic relaxation may further affect sorption energetics and influence the degree of cation hydration near the surface. Interfacial relaxation has been assessed both theoretically (Odelius et al., 1997; Steele et al., 2000) and experimentally (Hartman et al., 1990; Wicks et al., 1993; Henderson et al., 1994; Vrdoljiak et al., 1994; Kuwahara, 1999, 2001; Cheng et al., 2001) with variable results. Odelius et al. (1997) and Steele et al. (2000) predicted, from first principle molecular dynamics and classical molecular dynamics, respectively, that muscovite layers with sorbed K, Cu, Zn, and Cd would undergo little relaxation, but they did not quantify the extent of this relaxation. Kuwahara (2001) used atomic force microscopy (AFM) images to conclude that the oxygens of the muscovite basal planes exposed upon cleavage are not at the same vertical position. This surface corrugation is consistent with that of the bulk crystal structure. However, the lateral uncertainties in atom positions determined from AFM images are larger than the expected changes in bond distances due to relaxation. Cheng et al. (2001) observed substrate relaxations of muscovite immersed in deionized water using high-resolution X-ray reflectivity and found displacements of <0.04 Å in the outermost polyhedral layer with relaxations in deeper layers having a typical magnitude of 0.01 Å.

3. Materials and methods

3.1. Muscovite origin and bulk structure refinement

A natural muscovite, with nominal composition $KAl_2(Si_3Al)O_{10}(OH)_2$, and labeled ASTM-V1 "scratch free" grade, was obtained from Asheville Schoonmaker Mica Company. Crystals were 25.4×25.4 mm (1×1 in.) square by 0.2 mm thick. The bulk crystal structure was refined in order to obtain a set of reliable atomic positions to minimize any systematic errors of the derived surface structure associated with uncertainties in the bulk crystal structure. Several crystal discs ~200 μm in diameter and ~150 μm in thickness were cut out of a single square and checked for quality and stacking disorder on an X-ray precession camera. This analysis verified that the muscovite was of $2M_1$ polytype. The crystal showing the best diffraction pattern (i.e., sharpest and most regular diffraction spots) was mounted onto a Bruker P4 four-circle diffractometer equipped with a Mo rotating anode generator and fitted with an incident beam graphite monochromator to select Mo Kα radiation. The muscovite cell parameters were determined from the centered positions of 25 reflections in the range $8° \leqslant 2\theta \leqslant 30°$. The crystal structure was refined from intensity data collected at 50 kV and 200 mA for Miller indices $h \pm 8$, $k \pm 14$, and $l + 32$, resulting in a total of 4349 reflections, of which 2073 were unique. The data were reduced and corrected for Lorentz and polarization effects, resulting in 1799 unique reflections having intensities $>2\sigma(I)$. An analytical absorption correction was applied using the indexed shape and measured dimensions of the crystal (Sheldrick, 1997). The structure was refined in space group $C2/c$ using neutral-atom scattering factors from the International X-ray Crystallographic Tables (1973), and initial atom positions of Smyth et al. (2000).

3.2. Sample preparation for X-ray reflectivity

Electrolyte solutions with cationic concentrations of 0.01 m K^+ (pH 5.7), Cs^+ (pH 5.7), Ca^{2+} (pH 5.6), and Ba^{2+} (pH 5.3) and 0.5 m K^+ (pH 5.7), Cs^+ (pH 5.7), and Ca^{2+} (pH 5.5) were prepared by dissolving ACS reagent grade ($BaCl_2$, CsCl) or high purity grade ($CaCl_2$, KCl) salts in deionized water bubbled with high purity Ar(g). Muscovite sheets were cleaved on both sides with adhesive tape, and immediately immersed vertically in 50 mL centrifuge tubes filled with solution. Each sheet was reacted for at least one-half hour to ensure complete exchange of surface K^+ with solution cations (Xu and Salmeron, 1998). The samples were then mounted in a thin-film cell, wetted with additional solution, and covered with an 8 μm-thick Kapton film (Fig. 2). Capillary forces between the mica surface and the Kapton film maintained the presence of a few micrometers of solution above the surface (Fenter et al., 2000a).

3.3. X-ray reflectivity measurements

Specular X-ray reflectivity was measured in-situ at beamlines 12-BM, 12-ID-D (0.5 m CsCl), and 11-ID-D (0.5 m KCl) (BESSRC-CAT) of the Advanced Photon Source at Argonne National Laboratory. Most of the data were obtained at 12-BM, where a wavelength of $\lambda = 0.6349$ Å was selected with a Si (1 1 1) monochromator

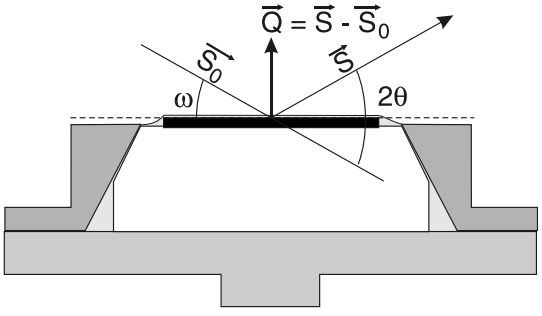

Fig. 2. Schematic representation of the thin-film cell and experimental reflectivity geometry. The incident and reflected X-ray beams are located in a plane perpendicular to the sample surface. The X-ray beam is reflected at the specular reflection condition $\omega = 2\theta/2$. $\mathbf{S}_0$ and $\mathbf{S}$ are unit vectors giving the direction of the incident and reflected beams, and $\mathbf{Q} = 2\pi(\mathbf{S} - \mathbf{S}_0)/\lambda$ is the momentum transfer vector.

and the X-ray beam was focused with a Rh-coated torroidally bent mirror, resulting in an incident beam cross-section of 0.2 mm (vertical) by 1 mm (horizontal) having an incident flux of $\sim 10^{10}$ photons/s. Measurement of high-quality reflectivity data relies on careful selection of the reflecting area, identified by rocking-curve scans approaching Gaussian-like shapes with resolution-limited widths (Fig. 3). Reflecting areas were approximately 1 mm wide, but varied in length from 12 to 0.7 mm over the range of angles studied. The optics were similar at the other beamlines except that a cylindrically bent Pd-coated mirror was used at 12-ID-D, and a (220) monochromator and a Pd-coated torroidally-bent mirror were used at 11-ID-D. The X-ray beam at these two beamlines had 10 to 100 times more useful photon flux allowing data to be obtained faster. The X-ray flux reflected by the (001) cleavage surface was measured as a function of the momentum transfer $Q = (4\pi/\lambda)\sin(2\theta/2)$, where 2θ is the angle between the incident and reflected beams, by rocking the crystal through the specular reflection condition. Reflectivities were determined by integrating peak areas after subtracting the background signal due, for example, from scattering by the solution layer. The reflectivity at two reference points was measured periodically to monitor the stability of the interfacial and bulk structure during data acquisition. For measurements performed with insertion device (ID) beamlines with a substantially larger incident flux ($\sim 10^{11}$ to 10^{12} photons/s), minor discoloration of the muscovite occurred within the X-ray beam footprint during the longer measurement periods (>5 h). However, no apparent changes in reflectivity due to sample irradiation were observed. Similar discoloration on orthoclase-water (Fenter et al., 2000a, 2003) and quartz–water (Schlegel et al., 2002) interfaces was thought to be due to the activation of color centers in the bulk crystal, which has no influence on the interface structure.

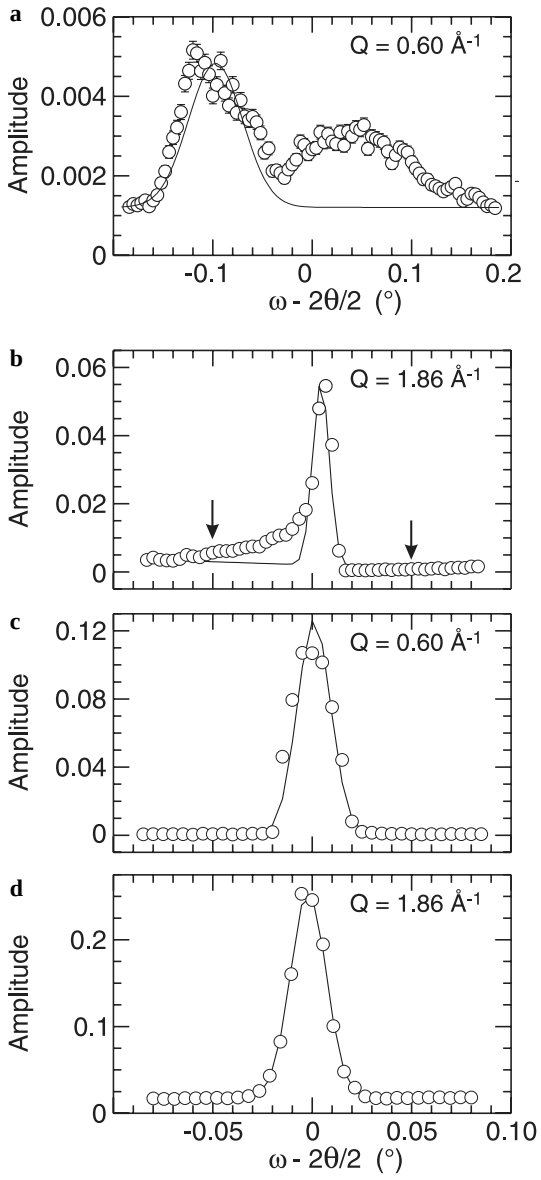

Fig. 3. Examples of rocking-curves collected at the muscovite-water interface. Samples with significant mosaic structure may have (a) two broad peaks, and/or (b) a single peak with a significant 'tail' at low angles which could be misinterpreted as a sloping background at different levels on either side of the peak (indicated by arrows). (c and d) Ideal detector slit-limited rocking curves at the same values of Q shown in (a) and (b) each displaying a single maximum above a flat background. Lines are Gaussian fits to the data.

Experimental reproducibility was checked by repeating selected experiments with different crystals and fresh solutions. Most experiments were performed on separate muscovite crystals, because only a small area devoid of significant mosaicity and imperfect surface cleavage could be obtained. Multiple measurements were performed on a single muscovite crystal for a few samples. In one case, we assessed cation exchangeability under the thin film of solution (Fig. 4). A 0.01 m $CaCl_2$ solution was replaced above a muscovite crystal by flowing about 20 mL of a 0.01 m $BaCl_2$ solution through the cell, and then again a 0.01 m $CaCl_2$ solution, with equilibration times typically >30 min prior to measuring the X-ray reflectivity. In the first $CaCl_2$ solution, a full set of data was measured. In each of the latter two solutions, reflectivity at selected values of Q was measured. Because a single muscovite sheet was used in this experiment, we avoided any uncertainties due to substrate variability.

Reflectivity data were modeled using atomistic structures that include a fixed bulk muscovite structure, relaxation of muscovite atomic positions near the surface, surface roughness, and structured layers of ions and molecules above the interface, capped by bulk water (Fenter et al., 2000a). Reflectivity as a function of momentum transfer, $R(Q)$, is expressed analytically by

$$R(Q) = (4\pi r_e/QA_{uc})^2 \left| \sum_j f_j \exp(iQz_j) \exp[-0.5(Q\sigma_j)^2] \right|^2, \quad (1)$$

where $r_e = 2.818 \times 10^{-5}$ Å is the classical electron radius, A_{uc} is the area of the unit cell in the ab plane

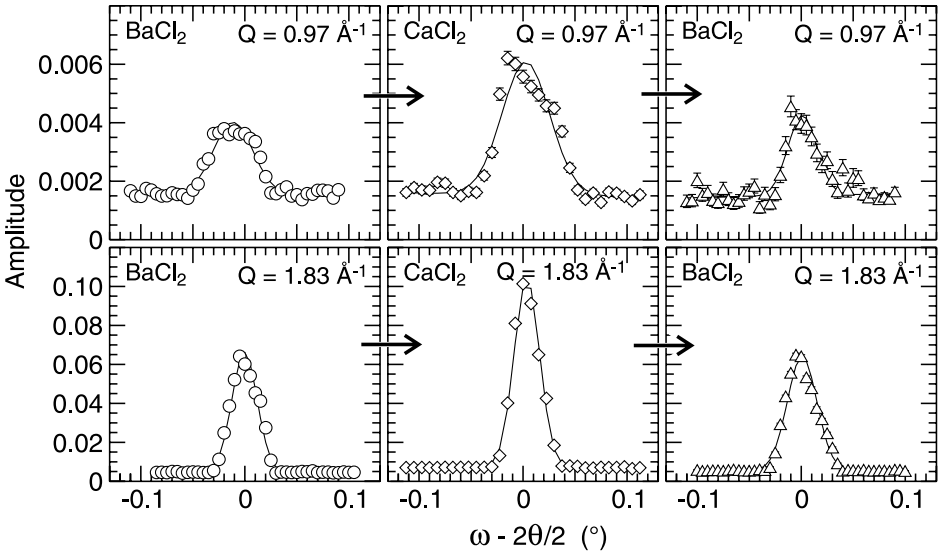

Fig. 4. Evolution of the amplitudes of rocking-curves at selected points with changes in the cationic composition of the solution. Muscovite was contacted with (from left to right) 0.01 m $BaCl_2$, then 0.01 m $CaCl_2$, and again with 0.01 m $BaCl_2$. The rocking curve amplitudes are fully recovered after the last solution change.

($A_{uc} = 46.72$ Å^2), and f_j, z_j and σ_j are the atomic scattering factor, position, and Debye–Waller parameter of the j^{th} atom. The sum in Eq. (1) is taken over all individual atoms per A_{uc} at the muscovite-water interface (i.e., muscovite structural oxygens and cations, sorbed cations and water, and water molecules in layers above the surface). Various models with different solution interfacial compositions were tested and resulted in essentially identical electron density profiles. Thus, the primary sensitivity of the data is to the electron density profile, and not to the atoms used in its model. Indirect sensitivity to the interfacial composition is achieved only by enforcing electroneutrality and steric constraints (e.g., the number density of water).

The resolution L of the data is a function of the reciprocal domain covered by the reflectivity measurements, and is approximately equal to π/Q_{max}, where Q_{max} is the highest Q value at which data were obtained (Fenter, 2002). A typical resolution, $L \sim 0.7$ Å for $Q_{max} = 5$ Å^{-1}, implies that sorbed species at the mineral–water interface can be detected as individual layers of ions and molecules along the surface normal direction. Charge compensation by cations is described as monolayer (ML) coverage where 1 ML = 1 ion/A_{uc}. For a monovalent cation, 1.0 ML would equal the permanent negative charge on the basal surface. For a divalent cation, the negative charge would be satisfied by 0.5 ML.

Because of the finite resolution of the data, coupled with the small relaxations expected for muscovite, we minimized the number of degrees of freedom of the fit wherever possible. We related the relaxation parameters for Si and Al in the muscovite sheets to relaxation of the oxygens to which they are bonded. Thus, with the notation used in Fig. 1a:

$$\delta(\mathrm{Si,Al})_{\mathrm{tet,high}}(i) = \frac{\delta(\mathrm{O})_{\mathrm{tet,high}}(i) + \delta(\mathrm{O,OH})_{\mathrm{oct,high}}(i)}{2}, \quad (2a)$$

$$\delta(\mathrm{Al})_{\mathrm{oct}}(i) = \frac{\delta(\mathrm{O,OH})_{\mathrm{oct,high}}(i) + \delta(\mathrm{O,OH})_{\mathrm{oct,low}}(i)}{2}, \quad (2b)$$

$$\delta(\mathrm{Si,Al})_{\mathrm{tet,low}}(i) = \frac{\delta(\mathrm{O,OH})_{\mathrm{oct,low}}(i) + \delta(\mathrm{O})_{\mathrm{tet,low}}(i)}{2}, \quad (2c)$$

where, for example, $\delta(\mathrm{Al})_{\mathrm{oct}}(i)$ is the relaxation parameter for octahedral Al in the i^{th} layer, and "i" increases into the bulk crystal, with $i = 1$ for the outermost tetrahedral-octahedral-tetrahedral (TOT) layer. The two layers closest to the muscovite surface (i.e., containing both sorbed cations and surface water) were modeled with independent heights, composition, and density. Above the surface and near-surface layers, the distribution of water molecules was constrained with a layered water model in which each layer was assumed to have the density corresponding to liquid water and the position and spacing of each layer is determined by only three parameters, namely the distance between successive layers, the Debye–Waller factor of the first layer (σ_{W1}), and a parameter describing the increase in Debye–Waller factor between successive layers ($\delta\sigma_W$) (Magnussen et al., 1995; Cheng et al., 2001).

The fit quality was evaluated by the reduced χ factor $\chi^2 = (1/n)\sum_Q[(R(Q)_{exp} - R(Q)_{calc})/\sigma(Q)_{exp}]^2$, where n is the number of independent data points, $R(Q)_{exp}$ and $R(Q)_{calc}$ are the experimental and calculated reflectivities, and $\sigma(Q)_{exp}$ is the experimental uncertainty on $R(Q)_{exp}$ resulting from X-ray counting statistics. The χ^2 value gives a quantitative measure of the total error per data point for a given model, and approaches 1 when a model reproduces the data within statistical uncertainty. From the least-squares fitting procedure, well-defined estimates for

the statistical uncertainty associated with model structural parameters are obtained. Uncertainties at the 95% (2σ) confidence level are reported for each parameter. A ratio of three to five data points per fitted parameter typically is required to determine a structure uniquely and this was achieved for all fits (Fenter, 2002). Unless explicitly stated, parameter values with no reported uncertainty were fixed during the fitting procedure. The most commonly fixed parameters were Debye–Waller factors, because they are usually poorly constrained by the data. Previous experience has shown that specifically adsorbed species tend to have small root mean-square (rms) widths (~0.1 to 0.2 Å) consistent with that observed for lattice atoms, while larger rms widths are observed for fluid-like layers adjacent to mineral surfaces (Fenter, 2002). The derived structures corresponding to the best-fit models are shown as 'resolution-broadened' electron density profiles in which the intrinsic profile corresponding to the model is broadened by a term characteristic of the experimental resolution. This broadening highlights those features that can expected to be uniquely determined from the experimental data as described in Fenter et al. (2001) and Fenter (2002).

4. Results

4.1. Bulk muscovite structure

Unit cell parameters and atomic positions for the bulk muscovite structure (Tables 1 and 2) are in good agreement with previous results (Bailey, 1984). The final structure refinement yielded a figure of merit $R(F) = \Sigma [| F_{obs} - F_{calc} | / F_{obs}]$ of 0.045, where F_{obs} and F_{calc} are observed and calculated structure factors. The weighted R-value was 0.040 and the goodness of fit was equal to 2.62. From the electron density map, it was possible to determine the position of hydrogen in the muscovite hydroxyl groups. The calculated K^+ occupancy in the interlayer sites equals 0.935(4), a value significantly lower than the value of 1 expected for a stoichiometric crystal. This discrepancy may be explained by the presence of lighter cations (e.g., H_3O^+, or Na^+) substituting for K^+ in the muscovite interlayer. The mean cation–oxygen distances for tetrahedral sites T1 and T2 are 1.643(2) and 1.646(2) Å, respectively. These values are equal within error, indicating that Si and Al are disordered in the tetrahedral sites.

Table 1
Unit-cell parameters for the $2M_1$ muscovite

a (Å)	5.1872(5)	α	90.00°
b (Å)	9.0070(12)	β	95.804(12)°
c (Å)	20.0592(31)	γ	90.00°

4.2. Rocking curves

The selection of a good reflecting area was necessitated by the mosaic structure of muscovite crystals (Holzer et al., 1998) and by the relative weakness of interlayer bonds. For example, rocking-curve scans frequently displayed two or more peaks (Fig. 3a), a consequence of the beam footprint covering adjacent domains of significant out-of-plane misorientation. Other scans displayed what appears to be a single peak, but with an apparent background at different levels on either side due to an asymmetric mosaic distribution attributed to curling of the surface layer resulting from imperfect cleaving (Fig. 3b). In each experiment the sample was moved until an area wider than the beam footprint could be found for which rocking curves had flat featureless background levels and approached reasonable Gaussian shapes, with resolution-limited widths at all Q values (Fig. 3c and d). Since the integrated surface reflectivity is independent of the mosaic structure, the best samples had rocking curves that were both narrower and more intense so that the intrinsically weak surface reflectivity could be more easily measured, as seen in Fig. 3. The presence of significant X-ray reflectivity over a broad range of Q, coupled with the absence of evidence for diffuse scattering near the specular direction (e.g., broadening of the rocking-curve peak, or presence of tails near Bragg peaks) confirmed that the targeted area was molecularly smooth with minimal mosaic structure.

Table 2
Atom position and thermal displacement parameters for the $2M_1$ muscovite

Site	x/a	y/b	z/c	occ	U_{11}[a]	U_{22}[a]	U_{33}[a]	U_{12}[a]	U_{13}[a]	U_{23}[a]	U_{eq}[a]
K	0.00	0.09886(10)	0.25	0.935(4)	2.19(4)	2.21(4)	2.27(4)	0.00	0.23(3)	0.00	2.223(23)
M2 (Al)	0.25023(11)	0.08345(7)	0.00004(3)	1.017(4)	0.57(3)	0.64(3)	1.05(3)	−0.04(2)	0.08(2)	0.03(2)	0.752(15)
T1	0.46521(11)	0.92979(6)	0.13544(3)	Si: 0.75 Al: 0.25	0.61(2)	0.63(2)	1.14(3)	−0.03(2)	0.09(2)	0.05(2)	0.792(14)
T2	0.45127(11)	0.25844(6)	0.13544(3)	Si: 0.75 Al: 0.25	0.62(2)	0.68(2)	1.13(3)	0.03(2)	0.06(2)	0.04(2)	0.811(14)
O1	0.41602(32)	0.09292(18)	0.16846(8)	1.0	1.81(7)	1.09(6)	1.57(7)	−0.01(6)	0.40(6)	0.03(6)	1.471(40)
O2	0.25139(31)	0.81054(19)	0.15763(9)	1.0	1.20(7)	1.79(8)	1.95(8)	−0.32(6)	0.00(6)	0.43(7)	1.655(44)
O3	0.24964(30)	0.37088(19)	0.16895(9)	1.0	1.31(7)	1.54(7)	1.68(8)	0.44(6)	−0.06(6)	−0.15(6)	1.523(42)
O4	0.46177(27)	0.94409(17)	0.05348(8)	1.0	0.79(6)	1.01(6)	1.27(7)	0.12(5)	0.04(5)	0.04(6)	1.028(36)
O5	0.38368(28)	0.25142(16)	0.05359(8)	1.0	0.96(6)	0.91(6)	1.23(6)	0.03(5)	0.01(5)	0.05(6)	1.054(36)
O6 (OH)	0.45835(29)	0.56114(18)	0.05002(8)	1.0	1.02(6)	1.02(6)	1.53(7)	−0.05(5)	0.28(6)	−0.21(6)	1.180(39)
H	0.394(9)	0.629(5)	0.057(2)	1.0	6.0(1.4)						

[a] ×100.

4.3. Reflectivity data

Specular reflectivity data were measured to $Q \geqslant 4$ Å^{-1} for all systems (Figs. 5–8). Plots of the specular X-ray reflectivities as a function of Q all follow the expected form of a crystal truncation rod (CTR), in which the intensity is largest near the bulk Bragg reflections but decreases continuously to values as low as 10^{-9} between bulk Bragg peaks (Figs. 5–8a). Normalized reflectivity data were obtained upon dividing by the generic form of a CTR, $R_{ctr} = 1/(Q\sin(Qd_{\perp}/2))^2$, where $d_{\perp}$ is the substrate layer spacing (in this case equal to d_{002} of muscovite). This normalization makes it easier to see more subtle features of the data (Figs. 5–8b).

Reflectivity data in 0.01 m KCl and CsCl solutions show conspicuous differences in reflected amplitude as a function of Q (e.g., at $Q \approx 1.0$, 1.75, and 2.6 Å^{-1}; Figs. 5,6). These differences are due to the presence of surface-associated cations with significantly different numbers of electrons (i.e., K^+ with 18 e^- and Cs^+ with 54 e^-). Reflectivity data collected in 0.01 m $BaCl_2$ and $CaCl_2$ also differ in shape and amplitude, e.g., at $Q \approx 1.6$, 2.6 and 3.6, and 4.2 Å^{-1} (Figs. 7 and 8), although the differences are not as pronounced as for the monovalent cations. The cation exchange test using 0.01 m $CaCl_2$ and $BaCl_2$ showed that observed changes in reflectivity at selected Q values, however, are reversible (Fig. 4) and match the differences in integrated intensities from the full CTRs on distinct samples reacted in these two solutions. Thus, although the differences in the 0.01 m $CaCl_2$ and $BaCl_2$ CTRs appear to be relatively small when plotted in Figs. 7 and 8, they are significant and reproducible, and cannot be attributed to differences in crystal substrate reflectivity. Also, reflectivity data recorded on separate samples of muscovite immersed in 0.01 m $BaCl_2$ are equal within statistical error, confirming that the experiments are reproducible and the data reflect the intrinsic structure of the cation-sorbed muscovite-water interface (Fig. 8). Only small differences in amplitude can be observed between reflectivity data collected in either 0.01 or 0.5 m KCl (Fig. 5) or 0.01 and 0.5 m $CaCl_2$ (Fig. 7). However, changing the concentration of the CsCl solution resulted in large differences in the data (Fig. 6).

4.4. Solid surface structure

The best fits to reflectivity data were obtained by allowing relaxation of muscovite atomic layers to propagate into the solid, from ~30 Å (0.01 m and 0.5 m CsCl, 0.01 m KCl) to ~40 Å (0.5 m KCl, 0.01 and 0.5 m $CaCl_2$, 0.01 m $BaCl_2$; Fig. 9). However, relaxation parameters were generally modest. In most cases, a small displacement of the interlayer structural cation was observed. For example the maximum vertical displacement of structural K^+ with respect to its unrelaxed position ($\delta K = 0.06(3)$ Å) was found for 0.01 m KCl, 0.5 m CsCl, and 0.5 m $CaCl_2$. These values are smaller than the

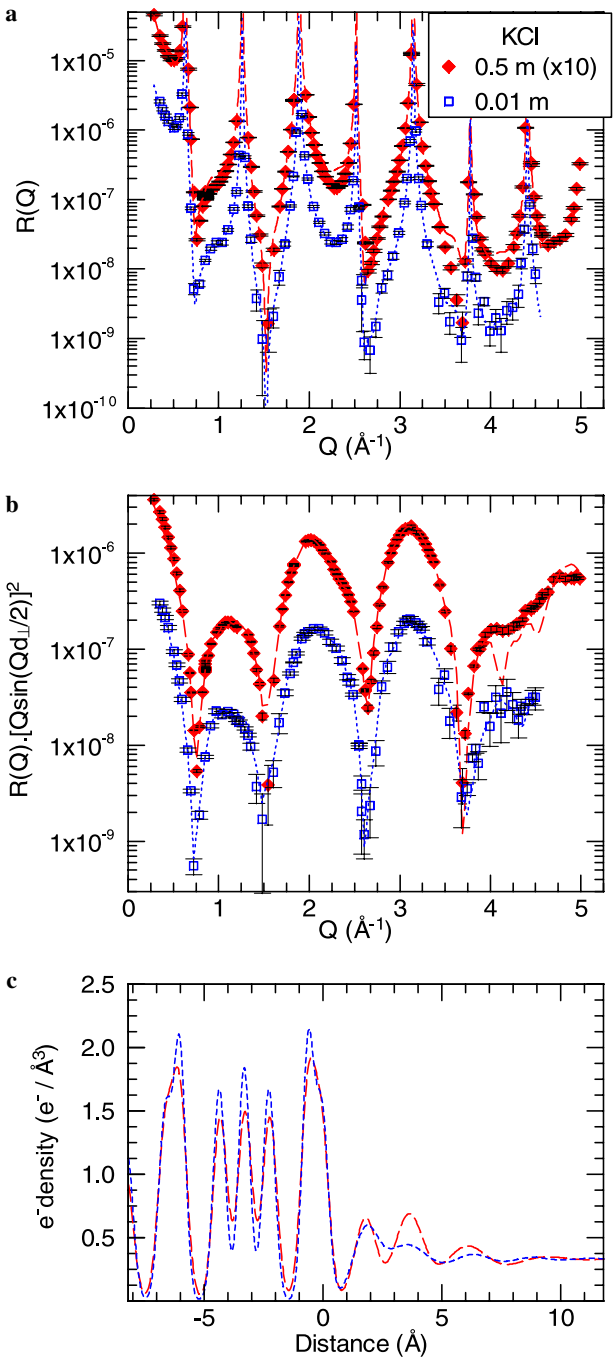

Fig. 5. (a) Reflectivity data for muscovite in 0.01 m (□) and 0.5 m (◇) KCl. Also shown are the best-fit model curves for 0.01 m (dotted line) and 0.5 m (dashed line) KCl. Only the tails of the Bragg peaks are shown. (b) Normalized reflectivity data $R(Q)[Q\sin(Qd_{\perp}/2)]^2$ (where $d_{\perp}$ is the vertical distance between two muscovite layers) and best-fit models. Same symbols as in (a). (c) Plots of the laterally-averaged electron density profiles in the direction normal to the surface for 0.01 m (dotted line) and 0.5 m (dashed line) KCl, as obtained from the best-fit results. The point marked 0 Å represents the hypothetical position of surface K^+ as if it were in the bulk crystal structure. Positive distances indicate solution structure and negative distances indicate the solid structure.

Debye–Waller parameter for bulk K measured along the [001] direction (0.139 Å). Only slight dissimilarities can be observed among relaxation profiles obtained for

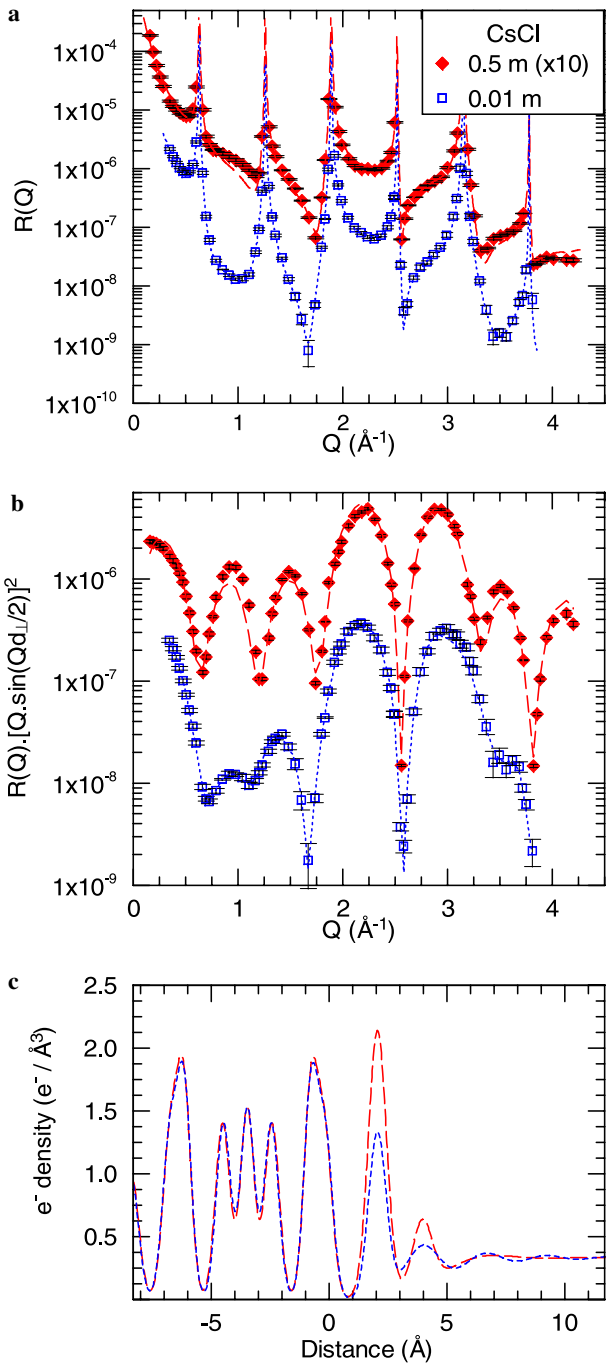

Fig. 6. (a) Reflectivity data (symbols) and best fits (lines) for muscovite in 0.01 m (□, dotted line) and 0.5 m (◇, dashed line) CsCl. Only the tails of the Bragg peaks are shown. (b) Normalized reflectivity data $R(Q)[Q\sin(Qd_{\perp}/2)]^2$ and best-fit models. Same symbols as in (a). (c) Plots of the laterally averaged electron density profiles in the direction normal to the surface for 0.01 m (dotted line) and 0.5 m (dashed line) CsCl, as obtained from the best-fit results.

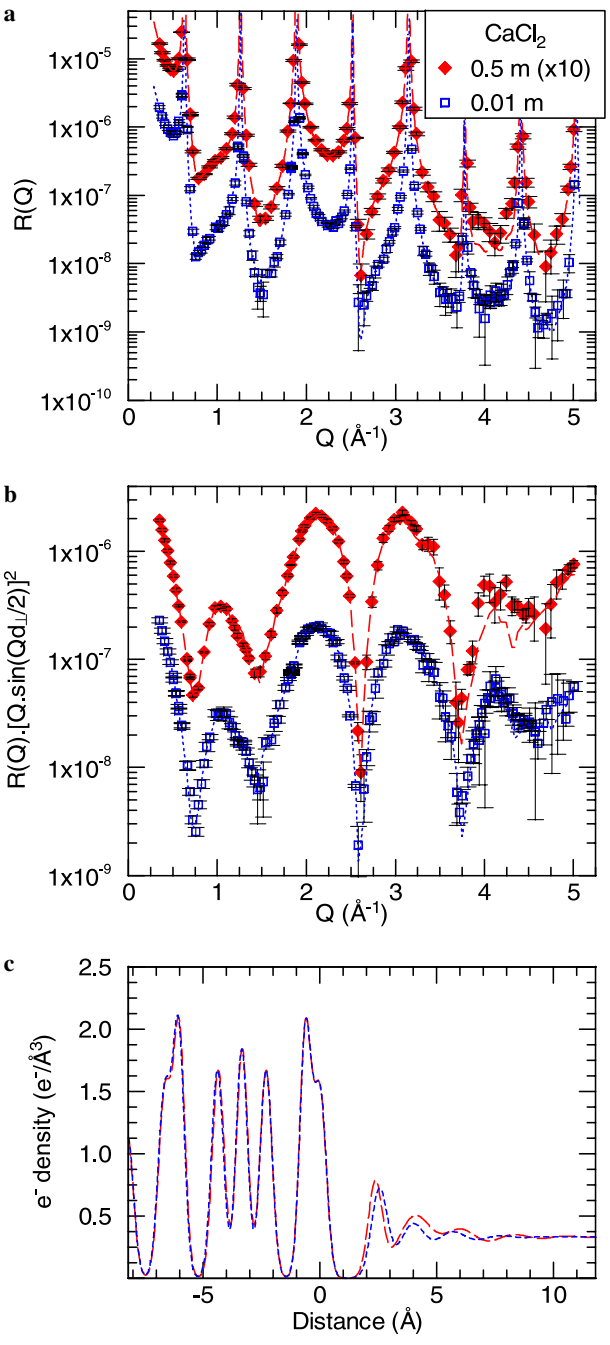

Fig. 7. (a) Reflectivity data (symbols) and best fits (lines) for muscovite in 0.01 m (□, dotted line) and 0.5 m (◇, dashed line) $CaCl_2$. Only the tails of the Bragg peaks are shown. (b) Normalized reflectivity data $R(Q)[Q\sin(Qd_{\perp}/2)]^2$ and best-fit models. Same symbols as in (a). (c) Plots of the laterally averaged electron density profiles in the direction normal to the surface for 0.01 m (dotted line) and 0.5 m (dashed line) $CaCl_2$, as obtained from the best-fit results.

distinct concentrations of the same electrolyte. For example, the relaxation of structural K^+ at a depth of −10 Å appears greater in 0.01 m KCl than in 0.5 m KCl (Fig. 9a). Comparable dissimilarities can be observed among relaxation profiles for 0.01 and 0.5 m CsCl, or for 0.01 and 0.5 m $CaCl_2$. Nonetheless, differences between relaxation parameters at the same structural level are generally <0.10(4) Å.

The rms surface roughness, evaluated using standard methods (Fenter, 2002; Schlegel et al., 2002), is ⩽2.3 Å, smaller than the height expected for surface steps (∼10 Å). This small roughness indicates that the muscovite surface is smooth at the molecular scale over large areas, as

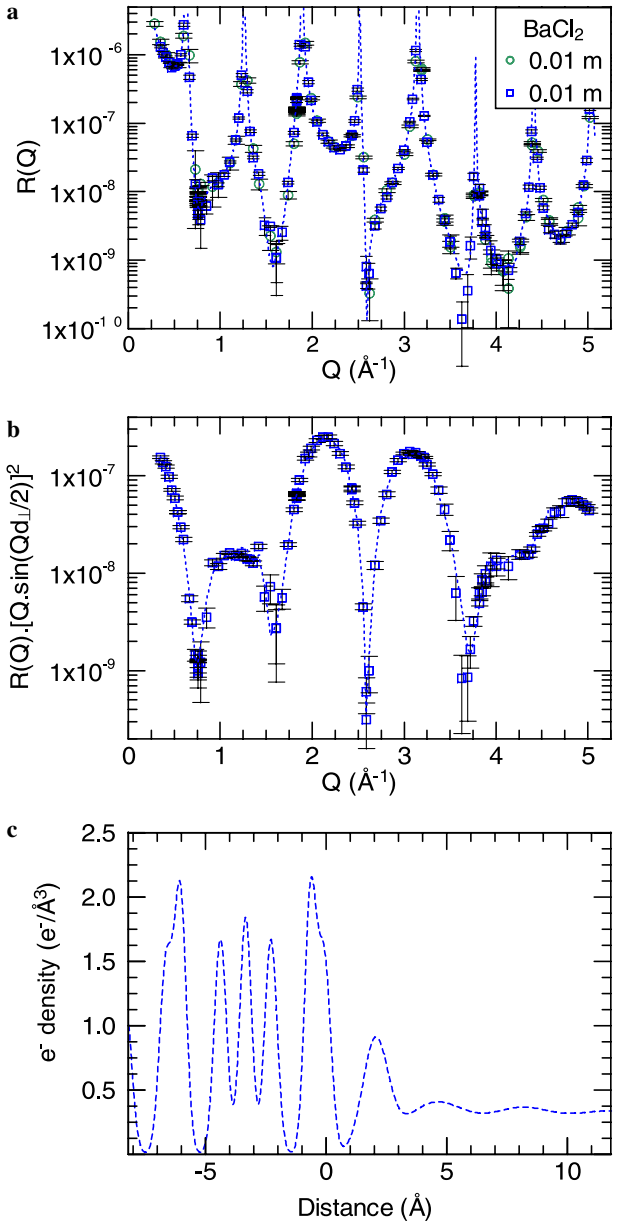

Fig. 8. (a) Overlay of the two data sets for muscovite in 0.01 m $BaCl_2$ (□,O), and best-fit model for the extended data set (dotted line). Only the tails of the Bragg peaks are shown. (b) Normalized reflectivity data $R(Q)[Q\sin(Qd_{\perp}/2)]^2$ and best-fit model. Same symbols as in (a). (c) Plots of the laterally averaged electron density profiles in the direction normal to the surface for 0.01 m $BaCl_2$, as obtained from the best-fit results.

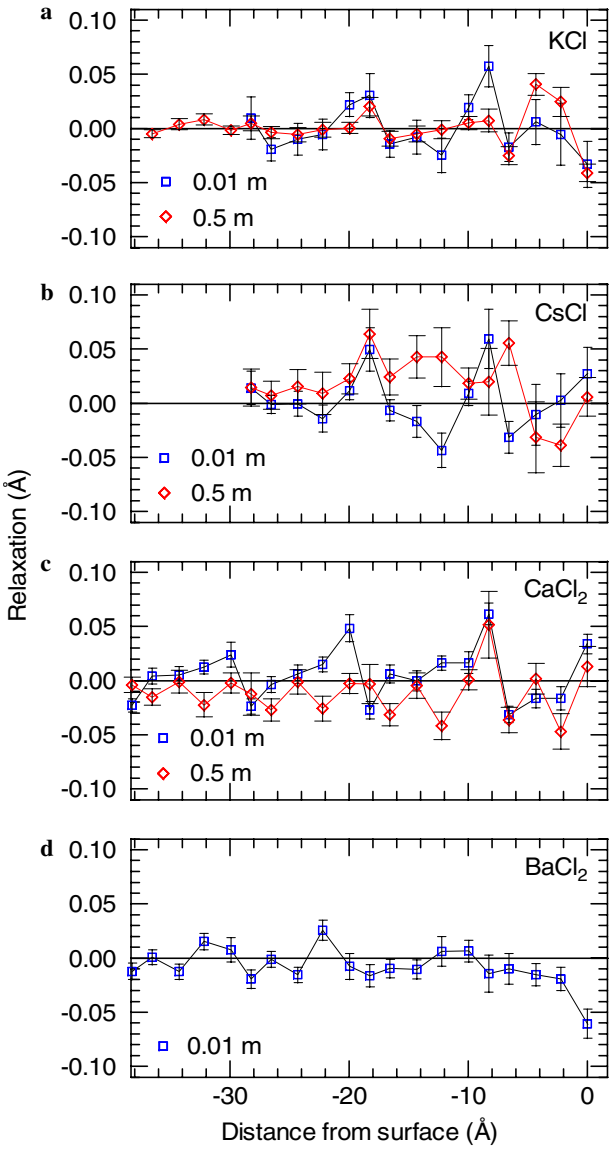

Fig. 9. Plots of the vertical relaxation for the four oxygen positions and the interlayer K^+ position as a function of distance from the surface, for (a) 0.01 and 0.5 m KCl, (b) 0.01 and 0.5 m CsCl, (c) 0.01 and 0.5 m $CaCl_2$, and (d) 0.01 m $BaCl_2$.

has been shown numerous times by atomic force microscopy (e.g., Kuwahara, 1999). A lower limit for the average lateral step spacing can be obtained from the width of the rocking curve, $\Delta\theta$, which in turn is related to the lateral width of the specular rod (i.e., parallel to the surface), $\Delta Q_{\parallel} = Q\Delta\theta = 2\pi/L$, where Q is the momentum transfer, and L is the domain size. Since the rocking curve width in these measurements is either resolution limited (i.e., limited by the detector slit size) or due to sample mosaic, this calculated value provides only a lower limit of the domain size. Using the observed rocking curve width of ~0.02° at $Q = 0.6$ Å^{-1}, we obtain $L > 3$ μm. The effect of surface roughness on experimental data can be described with a multiplicative factor in Eq. (1) expressed by a single parameter (Robinson, 1986). Any added uncertainty in the structure of the near-surface solution due to the surface roughness (or any other parameter used to describe the interfacial structure) is included in the derived statistical errors through parameter correlations.

4.5. Interfacial solution structure

We determined the interfacial electron-density profiles using many structural models that differed in terms of molecular composition and distribution within the first two layers of the solution (i.e., interfacial structure

described with only water, with individual layers modeled with a single cation, or with a combination of water and cations). However, each group of models for a given data set produced resolution-broadened electron density profiles in which the position and amplitude of peaks were reproduced within reported uncertainties, indicating that the derived profiles represent primarily the intrinsic electron density distribution regardless of each model's details. Thus, the main challenge, elaborated upon in the discussion, is to further constrain the distribution of atoms and molecules that compose the electron density profiles. Consequently, the interfacial structures will be discussed from the perspective of the derived electron density profiles.

All electron density profiles display oscillations in the solution that dampen away from the interface (Figs. 5–8c). The first peak, with the greatest electron density, is in the solution layer closest to the surface oxygens at a height $\geqslant 1.7$ Å above the surface, significantly farther than the surface water layer (1.3 Å) reported by Cheng et al. (2001). We attempted to split this first layer into two sublayers to more closely resemble the interfacial structure in deionized water (Cheng et al., 2001) but determined that the data were better explained by a single peak, which suggests that the layer's height truly reflects the distance between adsorbed species and the oxygen basal plane. The integrated electron density of the first peak increases with increasing atomic number for each pair of isovalent cations at the same bulk solution concentration (Table 3). For example, the integrated electron density in KCl solutions is about 40% of that in CsCl solutions of the same ionic strength. The increase in integrated peak area with increasing atomic number of the electrolyte cation suggests that a significant part of the electron density is due to the adsorbed cation. Also, there is an increase in the integrated electron density of the first layer with an increase in solution concentration for a given cation (Table 3). This concentration dependence, which is most pronounced for the 1:1 electrolytes, reveals a compositional change in the first layer, e.g., a change in the occupancy ratio of cations to water molecules.

For all systems, the increase in bulk solution concentration also coincides with a small apparent increase in the electron density peak for the next-nearest surface layer (Figs. 5–7c). However, the integrated electron density for this layer varies little with solution cation (as seen in Table 3), suggesting that these changes are primarily associated with changes in the shape of the electron density profile. Above these two surface layers, additional water layers are observed, at and above heights from 5.6(1) to 6.7(2) Å (Table 3). These water layers appear as damped oscillations in the electron density profiles (Figs. 5–8c). The periods of the oscillations vary from 2.3(2) Å in 0.01 m $CaCl_2$ to 3.0(1.3) Å in $BaCl_2$ (Table 3) and compare fairly well with the water molecular size (~2.7 Å; Cheng et al., 2001). The oscillations disappear at a distance of ~10 Å from the surface. There are no significant changes in the structural parameters of these outer layers as a function of cation concentration (Table 2) indicating that there is minimal occupation of these layers by the cations.

5. Discussion

Interpretation of the derived electron density profiles in terms of number and position of cations and water molecules requires different conceptual approaches. Overall, the derived electron density profiles for each data set can be characterized by a number of well-organized solution layers just above the muscovite surface. The differences in the present results with respect to the layered structure reported for the muscovite-water interface (Cheng et al., 2001) suggest that the interfacial hydration layer is disrupted, due to, for instance, the formation of ion hydration shells. Nonetheless, the simple layered water model used previously for the muscovite-water interface is generally successful at providing a quantitative description of the interfacial structure in electrolyte solutions.

The laterally averaged electron density profiles derived from the specular reflectivity data are not element-specific (Park et al., 2005) because the Q-dependencies of scattering factors for distinct elements are similar in shape. So, changes in the nature of interfacial species are easily offset by small variations in occupancy and Debye–Waller parameters in the model fitting. Furthermore, cation heights are inferred largely from changes in the derived electron

Table 3
Electron density parameters for the nearest (first) and next-nearest (second) solution layers above the muscovite surface, and structural parameters for water close to the muscovite surface

Solution	First solution layer		Second solution layer		"Solution" water		χ^2
Composition	Height (Å)	Integrated e^- density (e^-/A_{uc})	Height[a] (Å)	Integrated e^- density (e^-/A_{uc})	Height[a] (Å)	Period[b] (Å)	
0.01 m KCl	1.67(6)	23(6)	3.8(2)	45(5)	6.3(3)	2.7(3)	4.4
0.5 m KCl	1.77(7)	35(7)	3.6(9)	48(5)	6.0(3)	2.9(3)	15.6
0.01 m CsCl	2.15(9)	57(6)	4.0(2)	34(7)	6.3(3)	2.3(4)	2.2
0.5 m CsCl	2.16(2)	90(5)	4.0(1)	30(4)	6.7(2)	2.0(5)	7.7
0.01 m $CaCl_2$	2.46(5)	30(4)	3.8(2)	26(3)	5.6(1)	2.3(2)	3.1
0.5 m $CaCl_2$	2.56(11)	35(5)	4.2(2)	33(3)	6.1(2)	2.4(5)	3.8
0.01 m $BaCl_2$	2.02(5)	50(6)	3.8(5)	25(4)	5.7(5)	3.0(1.3)	2.9

[a] Measured with respect to basal plane oxygens.
[b] Period of the oscillations in electron density for bulk water.

densities, either for the same cation at different solution concentrations, or for similar cations at the same concentrations, taking into account electrochemical and structural constraints.

The first constraint is that the permanent negative charge of the muscovite must be balanced by cations either directly sorbed, i.e., located in the first one or two solution layers, or within a more distant diffuse ion profile (in more distant solution layers). The maximum number of sorbed cations (or cationic complexes) is then dictated by the muscovite negative charge, assuming that charge overcompensation is precluded. Sorption sites contributed by surface step edges are negligible compared to the amount of permanently charged sites on molecularly smooth terraces as demonstrated by the large average size of surface domains ($d_d > 3$ μm) that was estimated based on the rocking curve width. For example, if we assume that surface domains are bounded by parallel steps, and that two cations cannot sorb closer than a distance equal to the sum of their hydrated radii (i.e., $r_h \geqslant 6$ Å), then the density of basal plane and edge sites would equal $1/A_{uc} \sim 1/(47 \times 10^{-8}) = 2.1 \times 10^6$ sites μm^{-2}, and $1/(d_d * r_h) \sim 1/(3 * 6 \times 10^{-4}) = 550$ sites μm^{-2}, respectively. The absolute number of edge sites available is orders of magnitude smaller than the number of basal sites, or the derived cation coverages (see below), and so we can justifiably impose electroneutrality at the interface based only on the permanent negative charge.

The second constraint is that the surface must be wetted, i.e., the average volume density of water molecules over some region away from the surface must not deviate too much from that of bulk water, despite the layered structure near the muscovite surface. This steric constraint limits the total number of ions and molecules in the surface layers, and in fact, sets a lower limit to the number of possible cations in these layers. Below, both constraints are used to select the most probable model for the physical distribution of cations near the muscovite surface.

5.1. Adsorption of monovalent cations

5.1.1. Surface coverage and adsorption mechanism of monovalent cations

Determining cation sorption mechanisms requires knowing the location and amount of cations in the solution layers nearest the surface, but the weak dependence of scattering factor on atomic number precludes direct determination of these values. Here, we discuss distinct approaches for solving this problem.

Qualitatively, the observed increase in integrated electron density of the first layer (ρ_1) with increasing solution concentration implies that the composition of the layer changes. This increase in ρ_1 can result from a greater proportion of cations or from an increasing total number of species (cations, water). However, it is unlikely that the total number of chemical species deviates significantly due to the steric constraint. Most plausibly, the proportion of cations within the first surface layers increases with increasing electrolyte concentration, as indicated by the well-known collapse of modeled diffuse double layers.

The first approach to estimating cation surface coverage (N_{Cat} per A_{uc}) is to assume that the layer nearest the surface is occupied only by the monovalent cation, and so ρ_1 is accounted for by 1.2(3) K^+ A_{uc}^{-1} in 0.01 m KCl, 1.8(4) K^+ A_{uc}^{-1} in 0.5 m KCl, 1.0(1) Cs^+ A_{uc}^{-1} in 0.01 m CsCl, and 1.6(1) Cs^+ A_{uc}^{-1} in 0.5 m CsCl. The calculated coverages in 0.5 m solutions are above those required to balance surface charge, and so some electron density must belong to other species, i.e., water ($Z = 10$). When the number of K^+ or Cs^+ are constrained to compensate surface charge, i.e., by fixing the monovalent cation coverage at 1 ML (or $N_{cat} = 1$ ML), water coverages (N_W) of 0.4(6) and 1.6(7) H_2O A_{uc}^{-1} in 0.01 and 0.5 m KCl, respectively, and 0.2(6) and 3.5(5) H_2O A_{uc}^{-1} in 0.01 and 0.5 m CsCl, respectively, account for the remaining electron density. Using these values, the number of atoms plus water molecules in the first layer in 0.01 m solutions is unrealistically low compared to the number estimated for a water-like density, which is about 3–4 entities per A_{uc} for a solution layer approximately 2.3–3 Å thick (a typical separation distance between successive layers). Also, these numbers are significantly lower in 0.01 m than in 0.5 m solutions, which defies any reasonable explanation. Therefore, the number of cations in the first layer in 0.01 m solutions must be less than the maximum needed to balance the muscovite charge, and there must be a corresponding increase in the number of water molecules. Because cation and water contents co-vary, the number of cations cannot be determined directly without invoking another constraint.

A second way to estimate the number of cations at the surface is to assume that the total number density of species does not vary with ionic strength. In other words, the number density of entities in the first adsorbed layer in the 0.01 m solutions should be identical to that at the higher ionic strength, where the number of sorbed cations may be expected to be equal to 1 ML, based on the arguments presented above. In CsCl systems, a total of 4.5 entities per A_{uc} was obtained by assuming full charge compensation at 0.5 m, and so 0.2 Cs^+ A_{uc}^{-1} with 4.3 H_2O A_{uc}^{-1} are calculated from ρ_1 for 0.01 m CsCl. The presence of ~4.5 atoms per A_{uc} is consistent with the results of Cheng et al. (2001), who modeled the first adsorbed water layer as having four water molecules per A_{uc}. However, in 0.5 m KCl, ρ_1 can be accounted for by 1 K^+ A_{uc}^{-1} and 1.6 H_2O A_{uc}^{-1}, leading to a total of 2.6 ions and/or molecules, less than for the CsCl and pure water systems. In fact, in 0.01 m KCl, constraining the number of species to 2.6 per A_{uc} in the first layer yields a negative concentration of K^+, along with water. Therefore, it is insufficient to consider space-filling constraints only laterally within the first layer.

If we consider space-filling constraints over the volume of the first and second (ρ_2) layers ($A_{uc} * (\text{height}_{\text{solution water}} - \text{height}_{\text{layer1}})$) along with full charge compensation, we ob-

tain 6.4(1.2) and 6.5(0.9) H_2O A_{uc}^{-1} in 0.5 m KCl and CsCl, respectively, and volumes per entity of 27(3) Å^3 in 0.5 m KCl and 28(3) Å^3 in 0.5 m CsCl. These volumes are similar to the molecular volume in bulk water (29.9 Å^3). Extrapolating the total number density of molecular entities to low ionic strength, the density of surface cations in 0.01 m solutions equals −0.6(6) K^+ A_{uc}^{-1}, and 0.5(2) Cs^+ A_{uc}^{-1}, again indicating incomplete charge balance near the surface. Note that we have made no assumption about the actual sorption mechanism of the cations (i.e., inner-sphere versus outer-sphere retention).

An independent last method to estimate cation coverage is to assume that the differences in electron densities between profiles collected in CsCl and KCl solutions are due solely to the difference in atomic number ($Z_K = 19$ vs. $Z_{Cs} = 55$), i.e., there is an isomorphic substitution of cations with minimal changes to the interfacial water structure, and $[(\rho_1 + \rho_2)_{CsCl}] - [(\rho_1 + \rho_2)_{KCl}] = N_{Cat} * (Z_{Cs} - Z_K)$, where N_{Cat} is the number of cations in the surface layers. This calculation yields $N_{Cat} = 0.6$ ML in the 0.01 m solutions, and 1 ML in the 0.5 m solutions. Although these estimates have relatively large uncertainties (~30%), to first-order they demonstrate at least partial charge balance by the sorbed cations in 0.01 m solutions, and approximately full charge balance in 0.5 m solutions. However, there is still a deficit of water near the surface for the 0.01 m KCl solutions, if we assume that the solution density must approximate that of water.

The last approach (isomorphic substitution) provides the most reasonable results for surface coverage, and fulfills expectations that the substrate charge would be compensated at sufficiently high solution concentrations. The results are similar to that derived for Cs at 0.01 m when charge compensation was assumed at 0.5 m. The approach using space-filling constraints was inadequate to describe the adsorption of K at low ionic strength likely because of the relatively smaller fraction of electron density contributed by K.

5.1.2. Comparison of calculated coverages with estimates from diffuse double layer (DDL) theory

Some of the muscovite charge may be balanced by hydronium ions and/or ions in a diffuse ion profile, which would account for the cation deficit at low ionic strength. Here, we compare predictions from DDL theory to determine if experimentally-derived coverages are sensible. The amount of cations expected in a diffuse layer is calculated using classical Gouy–Chapman theory, and by difference an amount is determined for the near-surface region assuming overall full charge compensation. It is important to keep in mind that these calculated amounts will be lower limits for the actual surface coverage of K^+ or Cs^+ because DDL theory neglects chemical interactions between solution species and the surface as well as the reduced permittivity of water at a surface (Sposito, 1984). The amount of charge $\sigma(x)$ at a distance greater than z from a negatively charged surface is given for a monovalent electrolyte by (Sposito, 1984; Singh and Uehara, 1998)

$$\sigma(x) = \left[2\varepsilon\varepsilon_O RT \sum_i C_i \left(\exp\left(-\frac{Z_i F\psi(x)}{RT}\right) - 1\right)\right]^{1/2}, \quad (3)$$

where ε is the dielectric permittivity of water, ε_0 the dielectric permittivity in a vacuum, R the gas constant, T the temperature, F the Faraday constant, $\psi(z)$ the potential at a distance z from the surface, Z_i and C_i the formal charge and the bulk solution concentration of the i^{th} species, and the summation is made over all solution species. $\psi(z)$ is expressed in a solution of monovalent ions by

$$\psi(x) = \frac{4RT}{F}\operatorname{atanh}\left[\tanh\left(\frac{F\psi(0)}{4RT}\right)\exp(-\kappa x)\right], \quad (4)$$

with

$$\kappa = \sqrt{\frac{2F^2 C_i}{\varepsilon\varepsilon_0 RT}}, \quad (5)$$

where the potential at the charged surface, $\psi(0)$, is a simple function of the surface charge σ_0 and equals (Singh and Uehara, 1998)

$$\psi(0) = \frac{2RT}{F}\operatorname{arcsin h}\left[\sigma_0 / \left(\frac{2C_i\varepsilon_0 RT}{\pi}\right)^{1/2}\right]. \quad (6)$$

The fractional amounts $(\sigma(x)/\sigma_0)$ of cations located beyond the point of maximum electron density in the second adsorption layer (3.8 Å for 0.01 m KCl and 4.0 Å for 0.01 m CsCl) are 0.30 and 0.28, corresponding to densities of adsorbed K^+ and Cs^+ in the first layer of 0.7 and 0.72 ML, respectively. These values are somewhat larger than those obtained from the space-filling and isomorphic-substitution calculations discussed above, but are less than the value of about 0.9 ML modeled from results obtained with the surface force apparatus (SFA) on opposing muscovite plates immersed in electrolyte solutions (Pashley, 1981). In 0.5 m solutions, $\sigma(x)/\sigma_0 \approx 0$, implying that all cations are in the first layer, as we had estimated, and as Pashley (1981) had modeled from SFA data.

5.1.3. Height of sorbed monovalent cations above the surface

Our estimates of surface coverage indicate that K^+ and Cs^+ adsorb mainly within the first layers, especially at high ionic strength. We now discuss the position of the first layer in terms of nominal cation height, keeping in mind that our analysis of adsorbed cation coverage revealed that part of the electron density is associated with water molecules.

The height of the first layer above the muscovite surface is smaller in KCl (~1.7–1.8 Å) than in CsCl solutions (2.1–2.2 Å). The greater height of Cs corresponds to its larger ionic radius (1.67 Å) compared to that of K^+ (1.38 Å) (Shannon, 1976). The height of the first layer in KCl is the same, within error, as the vertical distance between interlayer K^+ and oxygens of the siloxane basal planes (1.696 Å) in the bulk muscovite. The absence of vertical

relaxation with respect to the bulk position suggests that K^+ remains above the ditrigonal siloxane cavity at the free surface. This result contrasts with a recent ab initio study in which K^+ at the surface of muscovite exposed to water vapor relaxed to an adsorbed height of ~2 Å (Odelius et al., 1997). The higher value from Odelius et al. (1997) may be due to the limited number of water molecules in the ab initio modeling, and consequent undersaturation of water bonds. Also Monte-Carlo molecular modeling of K^+ adsorption on montmorillonite, a layered aluminosilicate similar to muscovite, but with an overall smaller (0.75 $e^- A_{uc}^{-1}$), and less localized permanent negative charge (0.25 and 0.5 $e^- A_{uc}^{-1}$ in the tetrahedral and octahedral sheets, respectively), suggested that K^+ should adsorb above the basal plane oxygens of substituted tetrahedra (Boek et al., 1995). The calculated minimum height of K^+ in this position, assuming oxygen radii of 1.33 Å, a K^+-oxygen distance of 2.71 Å (equal to the sum of the radii for K^+ and O^{2-}), and a sorption geometry in which K^+ sits in the middle of the oxygen triad in a close-packing arrangement is 2.23 Å, well above the measured height.

The vertical distance between Cs and the basal plane oxygens, inferred from the height of the first solution layer above the muscovite surface (2.15(9) and 2.16(2) Å in 0.01 and 0.5 m CsCl, respectively) is slightly higher than that measured between interlayer Cs and the oxygen basal plane in nanpingite (1.922 Å), a Cs-mica (Ni and Hughes, 1996). However, this distance is below the height of 2.58 Å for Cs if positioned directly above substituted tetrahedra. Therefore, the data strongly suggest that Cs^+, like K^+, is located predominantly in the ditrigonal cavity. This geometry results in direct binding of Cs^+ to the oxygens of the muscovite surface, with a cation–oxygen bond distance about 0.4 Å greater than the sum of the two atomic radii.

5.2. Adsorption of divalent cations

5.2.1. Surface coverage and adsorption mechanism of divalent cations

As for the monovalent cations, some water must be present with Ca^{2+} or Ba^{2+} within the first two surface layers. If the amount of sorbed divalent cation exactly compensates the permanent charge (e.g., $N_{Ca} = 0.5$ ML), then for the 0.01 m solutions, we obtain 0.5 Ca^{2+} A_{uc}^{-1} with 2.0(4) H_2O A_{uc}^{-1}, and 0.5 Ba^{2+} A_{uc}^{-1} with 2.2(6) H_2O A_{uc}^{-1} (Table 3). For 0.5 m $CaCl_2$ fixing N_{Ca} at 0.5 ML, we find 2.5(5) H_2O A_{uc}^{-1}. Because the second layer in $CaCl_2$ or $BaCl_2$ solutions is at about the same distance from the surface (from 3.8 to 4.2 Å) as in KCl or CsCl solutions (3.6 to 4.0 Å), i.e., at distances slightly smaller than the second layer in pure water (4.6 Å; Cheng et al., 2001), the first layer should also contain about three entities per A_{uc}, in order to fill space. This case is met in all three of the divalent cation solutions investigated.

Applying the volume space-filling constraints and assuming the presence of 0.5 ML of Ca^{2+}, we obtain 5.8(8) H_2O A_{uc}^{-1} in the first two layers at the surface. If the amount of water in these layers remains constant with ionic strength, the surface density of cation in 0.01 m solutions would equal (56(7) − 63(6))/(20 − 10) = −0.6(1.3) ML Ca^{2+} and (75(10) − 63(8))/(56 − 10) = 0.3(4) ML Ba^{2+}. It is difficult to draw a definite conclusion for Ca^{2+} given the uncertainties on the calculated occupancies. The calculated surface coverage for Ba^{2+}, however, suggests partial occupancy. Invoking the isomorphic substitution approach yields $N_{Cat} = 0.5$ ML in the 0.01 m solutions, or full compensation of the muscovite layer charge.

These derived surface coverages may be compared with those estimated from SFA measurements (Pashley and Israelachvili, 1984; Claesson et al., 1985; Pashley and Quirk, 1989). Pashley and Israelachvili (1984) developed a model for Ca^{2+}/H_3O^+ exchange, from which it can be calculated that the amount of Ca^{2+} adsorbed at pH ~5.7 in 0.01 m $CaCl_2$ is ⩾0.36 ML, enough to balance about 70% of the surface charge. Higher $CaCl_2$ concentrations favor more Ca adsorption.

Retention of Ca^{2+} or Ba^{2+} in the DDL may also result in a lower amount of cation in the first adsorbed layer. The amount of sorbed divalent cation may be estimated according to Eqs. (3) and (5), and by writing the surface potential as (Sposito, 1984)

$$\psi(x) = \frac{RT}{F} \ln\left\{\frac{3}{2}\tanh^2\left[\frac{\sqrt{3}}{2}\kappa x + a\tanh\left(\left[1 + 2\exp\frac{F\psi(0)}{RT}\right]^{1/2}/\sqrt{3}\right)\right] - \frac{1}{2}\right\}. \quad (7)$$

For 0.01 m Ca^{2+} or Ba^{2+}, $\sigma(x)/\sigma_0 = 0.12$ and 0.11 for diffuse layers at heights > 4.2 and 4.5 Å, respectively. In 0.5 m $CaCl_2$, $\sigma(x)/\sigma_0 < 0.04$, suggesting that cations would tend to adsorb in the first layer.

5.2.2. Height of sorbed divalent cations above the surface

The height of the first solution layer is greater in $CaCl_2$ solutions (2.46(5) to 2.56(11) Å) than in $BaCl_2$ (2.02(5) Å). The difference in heights is opposite in sign to the difference in the unhydrated cation radii ($r(Ca^{2+}) = 1.00$ Å; $r(Ba^{2+}) = 1.33$ Å). Values for hydrated radii from Robinson and Stokes (1959) ($r(Ca^{2+}_{hydr}) = 3.09$ Å, $r(Ba^{2+}_{hydr}) = 2.88$ Å) appear to be consistent with the sense of the difference. However, more recent values for the hydrated radii of Ca^{2+} and Ba^{2+} (3.18 and 3.23 Å, respectively) have the same relative ordering as the unhydrated crystallographic radii (Ohtaki and and Radnai, 1993).

If hydrated ions behaved like perfect spheres and adsorbed above ditrigonal siloxane cavities, then fully hydrated Ca would be located ~3.5 Å above the surface, far higher than the experimental height. At the measured height of 2.5 Å, a linear distance of about 1.3 Å is available between the bare Ca ion and basal O atom, too small to accommodate a water molecule, even above a ditrigonal cavity. The measured height of Ba^{2+} results in even less space than in the case of Ca^{2+}. This suggests that divalent cations

are only partially hydrated near the surface. The measured height of the first layer in the $CaCl_2$ solutions would allow Ca^{2+} to reside anywhere on the surface, not only above ditrigonal cavities, but also midway between two ditrigonal cavities, above the oxygen triad in a tetrahedron. In contrast, Ba^{2+}, at a height of 2.04 Å, would be too close to the surface to fit above the basal oxygens, and therefore should be associated only with the ditrigonal cavities.

The interpreted higher affinity of Ba^{2+} for sorption on ditrigonal cavities, compared to Ca^{2+}, is consistent with the relative hydration enthalpies of the two divalent cations. The value for Ca^{2+} (-1592 kJ mol^{-1}) is more negative than that for Ba^{2+} (-1304 kJ mol^{-1}), suggesting that Ca^{2+} may remain more hydrated and possibly more mobile at the muscovite surface than Ba^{2+}. Both hydration enthalpies are substantially more negative than those for K^+ and Cs^+ (-321 and -263 kJ mol^{-1}, respectively), which indicate weaker binding of water oxygens to the monovalent cations. The smaller magnitude of the hydration enthalpies and the close distances of the monovalent cations to the basal oxygen plane, which do not allow intervening water molecules, are evidence that these two cations sorb as classical inner-sphere complexes to the muscovite (0 0 1) surface, and may explain their high stability when compared to other sorbed ions on phyllosilicate surfaces in general (Jensen and Babcock, 1973; Bolt, 1979).

5.3. On the possibility of co-sorption of chloride with divalent cations

Many studies have reported that anions, particularly chloride, may cosorb with divalent cations on exterior surfaces of layered silicates or in interlayers of clays. For example, calcium and chloride were observed at the surface of muscovite reacted in $CaCl_2$ solution using X-ray photoelectron spectroscopy (XPS) (Xu and Salmeron, 1998). In contrast, only barium was measured by XPS after muscovite was contacted with aqueous $BaCl_2$ (Gier and Johns, 2000). Because XPS analyses are conducted ex situ under high vacuum, it is possible that the chloride observed by Xu and Salmeron (1998) was an artifact of sample preparation.

In clay–chloride solution systems, sorption of monovalent cation–chloride complexes ($MeCl^+$) has been inferred from spectroscopic, X-ray diffraction, and bulk sorption measurements. These measurements include $CdCl^+$ determined by nuclear magnetic resonance (Di Leo and O'Brien, 1999), $FeCl^+$ determined by Mossbauer spectroscopy (Charlet and Tournassat, 2005), and $CaCl^+$ determined by modeling XRD data (Di Leo and O'Brien, 1999; Ferrage et al., 2005) in the interlayer of a montmorillonite. Other divalent cations have been inferred to cosorb with Cl^- based on macroscopic sorption data (Sposito et al., 1983a,b; Tournassat et al., 2004). For example, Sposito et al. (1981) proposed adsorption of $CuCl^+$ on montmorillonite to explain copper retention in apparent excess of the cation exchange capacity. For cations that complex strongly with chloride such as Zn^{2+} or Cu^{2+}, competition between adsorption on exchange sites and fixation at clay edges can complicate interpretation of measured uptake in macroscopic sorption experiments (Schlegel et al., 2001). All of the above studies, but especially the results of Xu and Salmeron (1998) and Ferrage et al. (2005) on the $CaCl_2$ system, prompt evaluation of the in-situ X-ray reflectivity data with regard to the possible occurrence of $MeCl^+$ surface complexes.

In order for an $MeCl^+$ complex to reside at the surface, either there must be sufficient amounts in solution or the surface must stabilize their formation. The speciation of $CaCl_2$ and $BaCl_2$ solutions was calculated using Chess 2.4 (Van der Lee and DeVindt, 1999) with the EQ3/6 database (Wolery, 1992). In the 0.01 m solutions, Ca^{2+} and Ba^{2+} predominate (99.6% and 99.7% of dissolved cations, respectively), but concentrations of $CaCl^+$ and $BaCl^+$ (2.1×10^{-5} and 3.3×10^{-5} m, respectively) are high enough to have saturated the negative surface charge for the samples reacted in 50 mL of solution ($\sim4.3\times10^{-8}$ m of surface charge). In 0.5 m $CaCl_2$, the concentration of $CaCl^+$, calculated using Pitzer coefficients for the activity of ions in solution (Pitzer, 1991), is even higher ($\sim4.7\times10^{-3}$ m). Note that reduction of the solution dielectric permittivity near the interface would also favor the formation of ion pairs at the surface compared to the bulk solution.

Atomic positions above the surface of muscovite may be used to test for retention of metal chloride. If $CaCl^+$ adsorbs above the disiloxane cavity, the $CaCl^+$ radius of 2.35 Å (Raouafi et al., 1999) would result in a minimum height of 2.54 Å, which is close to the experimental value (2.46(7) Å). No experimental data exist for the radius of $BaCl^+$ to our knowledge. However, if the $BaCl^+$ radius increases by the difference between the crystallographic radii of Ca^{2+} (0.98 Å) and Ba^{2+} (1.33 Å) (Shannon, 1976), and therefore equals 2.70 Å, $BaCl^+$ could occur at a height of 2.88 Å, higher than the experimental height of 2.04(5) Å, but lower than the 3.26 Å height calculated for a spherical hydrated Ba^{2+} complex. We have assumed that the monovalent complex is a single entity with one radius. In reality, the complex of two atoms would be linear and the cation should approach the muscovite surface more closely. In this case, Cl^- would sit either directly above the divalent cation or at an angle to the surface normal direction closer to a structural oxygen atom. The latter position is less likely due to expected repulsion between anions.

The 0.5 m $CaCl_2$ electron density profile can be fit so that the first solution layer contains 0.95(14) ML of $CaCl^+$, exactly satisfying the permanent negative charge. In terms of space-filling constraints, however, 0.95 ML of $CaCl^+$ would result in no water molecules in the first layer and three water molecules in the second layer (Table 3). The $CaCl^+$ complex may be inferred to occupy the space of two water-like moieties, and so the total occupancy of the two layers would not deviate too much from the expected 6–7 entities per A_{uc}. In 0.01 m solutions, the electron density of the first layer is equivalent to 0.81(11) ML $CaCl^+$

and O.68(8) ML $BaCl^+$, making the total number density of entities in the first two layers even lower than in 0.5 m $CaCl_2$, clearly violating the space-filling constraints.

We conclude that adsorption of $CaCl^+$ complexes might account for some of the electron density profile in the 0.5 m solution, but the data are also consistent with sorption of uncomplexed Ca^{2+} at this concentration. In the 0.01 m $BaCl_2$ and $CaCl_2$ solutions, however, the results support the dominant sorption of uncomplexed cations.

5.4. Structure and relaxation of the solid surface

Relaxation of individual atomic layers was small (<0.07 Å), and decayed into the bulk structure through as many as four muscovite layers. Limiting the depth of the relaxation profile generally resulted in a significant increase in χ^2. For example, in 0.01 m $CaCl_2$, χ^2 increased from 3.1 to 6.7, 8.1, 10.0, and finally 13.3 as the number of fitted relaxed layers was decreased sequentially from four to zero. However, limiting the number of relaxed layers also increased the derived statistical errors on the fitted parameters of the relaxed layers. The depth of the relaxation profile that was needed to achieve the same magnitude of χ^2 generally decreased for the CsCl and $BaCl_2$ solutions. One explanation might be that the interface is stabilized to a slightly greater extent by a layer that is more electron dense than that of the interlayer cation.

Within the solid, the greatest atomic displacements affect interlayer K^+, similar to mica structural modifications effected by temperature (Guggenheim et al., 1987) or pressure (Catti et al., 1994; Comodi and Zanazzi, 1995). Relaxation of framework atoms close to the surface is limited when compared to relaxation of the wet surfaces of minerals such as gem-quality orthoclase (Fenter et al., 2000a), calcite (Fenter et al., 2000b), barite (Fenter et al., 2001), and quartz (Schlegel et al., 2002). The smaller displacements in muscovite may be due to the fact that the structural bonds cleaved in muscovite are weaker, because they are electrostatic in nature, than those broken by cleavage in the other minerals.

5.5. Water layering

Damped oscillations away from the surface were observed in the study of the muscovite-solution interface in pure water, and they were inferred to result from a "hard-wall" effect of the molecularly flat mica surface (Abraham, 1978). In this study, damped oscillations in the solution portion of the electron density profile were also seen in the model fits (Figs. 5–8c). The oscillation period approaches 2.5(2) Å, a value comparable to the water radius. Cheng et al. (2001) attributed the oscillations to water ordering in the direction normal to the surface. In the presence of sorbed cations, this water layering still exists, but its extent is slightly altered, presumably because the influence of the planar interface is decreased by the radial layering of water around sorbed cations.

6. Conclusions

High-resolution in-situ X-ray reflectivity data provide a new molecular-scale understanding of the structural properties of the interface between the layered silicate muscovite and aqueous salt solutions. The results show that vertical relaxation of atomic layers within the solid is limited (<0.07 Å), and decays into the crystal to depths of 30 to 40 Å. The greatest vertical relaxation in the solid is observed for atoms close to the surface and for interlayer K^+ ions. The water above the surface displays a density layering similar to that at the muscovite-water interface (Cheng et al., 2001), which was attributed to hard-wall effects at the molecularly flat basal surface.

An important aspect of the interfacial structure is the position of adsorbed cations at the muscovite-water interface. The closest approach of monovalent cations K^+ and Cs^+ to the uppermost oxygen atoms of the basal plane occurred at heights of 1.67(6) to 1.77(7) and 2.15(9) to 2.16(2) Å, respectively, close to the position of these cations in the bulk structure of micas. This suggests a relatively high degree of stability, and may explain the preferential adsorption of these cations on micas and clays in soils. Divalent cations Ca^{2+} and Ba^{2+} adsorbed closer to the muscovite (001) surface than they would if fully hydrated as in bulk solution, at distances of 2.46(5) to 2.56(11) and 2.02(5) Å, respectively. The distance of the first solution layer from the basal oxygen plane of muscovite in the divalent cation–chloride solutions suggests that calcium may remain more hydrated at the surface, but that barium is likely less hydrated and more tightly associated with the ditrigonal cavities. In the 0.01 m solutions for both monovalent and divalent cations, compensation of the surface permanent negative charge is incomplete within the first two solution layers (i.e., within distances above the muscovite surface of 3.6(9) to 4.2(2) Å) when constraints imposed by the solution density are considered, but is likely at least 50%, within the uncertainties. In the 0.5 m solutions, full compensation of this surface charge is achieved. The results also suggest that Ca^{2+} could exist, in part, as a $CaCl^+$ complex only at the higher ionic strength, but not in amounts needed to fully compensate the surface charge.

Acknowledgments

This study was supported by the Geosciences Research Program, DOE Office of Basic Energy Sciences, under Grants DE-FG03-99ER14979 to the University of Colorado, DE-FG02-02ER15364 to the University of Illinois at Chicago, and Contract W-31-109-Eng-38 to Argonne National Laboratory. Partial support was also provided by the National Science Foundation under grant EAR-990956 to the University of Colorado. The BESSRC team is thanked for technical assistance and for provision of

beamtime. We appreciate the careful reviews by R. James Kirkpatrick and an anonymous reviewer that were used in revising the manuscript.

Associate editor: Dimitri A. Sverjensky

References

Abraham, F.F., 1978. Interfacial density profile of a Lennard-Jones fluid in contact with a (100) Lennard-Jones wall and its relationship to idealized fluid-wall systems—Monte-Carlo simulation. *J. Chem. Phys.* **68**, 3713–3716.

Bailey, S.W., 1984. Crystal chemistry of the true micas. In: Bailey, S.W. (Ed.), *Micas*, vol. 13. Mineralogical Society of America, Washington, DC, pp. 13–60.

Bérend, I., Cases, J.-M., François, M., Uriot, J.-P., Michot, L.J., Masion, A., Thomas, F., 1995. Mechanism of adsorption and desorption of water vapor by homoionic montmorillonites: 2. The Li^+, Na^+, K^+, Rb^+ and Cs^+-exchanged forms. *Clays Clay Minerals* **43**, 324–336.

Boek, S.E., Coveney, P.V., Skipper, N.T., 1995. Monte Carlo molecular modeling studies of hydrated Li-, Na-, and K-smectites: understanding the role of potassium as a clay swelling inhibitor. *J. Am. Chem. Soc.* **117**, 12608–12617.

Bolt, G.H., 1979. *Soil Chemistry. B: Physico-Chemical Models*. Elsevier, Amsterdam.

Cases, J.-M., Bérend, I., François, M., Uriot, J.-P., Michot, L.J., Thomas, F., 1997. Mechanism of adsorption and desorption of water vapor by homoionic montmorillonites: 3. the Mg^{2+}, Ca^{2+}, Sr^{2+} and Ba^{2+}-exchanged forms. *Clays Clay Minerals* **45**, 8–22.

Catti, M., Ferraris, G., Hull, S., Pavese, A., 1994. Powder neutron diffraction study of $2M_1$ muscovite at room temperature and at 2 GPa. *Eur. J. Mineral.* **6**, 171–178.

Charlet, L., Tournassat, C., 2005. Fe(II)–Na(I)–Ca(II) cation exchange on montmorillonite in chloride medium: Evidence for preferential clay adsorption of chloride-metal ion pairs in seawater. *Aquatic. Geochem.* **11**, 115–137.

Cheng, L., Fenter, P., Nagy, K.L., Schlegel, M.L., Sturchio, N.C., 2001. Molecular-scale density oscillations in water adjacent to a mica surface. *Phys. Rev. Lett.* **87**, 156103.

Chorover, J., Amistadi, M.K., 2001. Reaction of forest floor organic matter at goethite, birnessite and smectite surfaces. *Geochim. Cosmochim. Acta* **65**, 95–109.

Claesson, P.M., Herder, P., Stenius, P., Eriksson, J.C., Pashley, R.M., 1985. An ESCA and AES study of ion-exchange on the basal plane of mica. *J. Colloid Interface Sci.* **109**, 31–39.

Comodi, P., Zanazzi, F., 1995. High-pressure structural study of muscovite. *Phys. Chem. Miner.* **22**, 170–177.

Davis, J.A., Kent, D.B., 1990. Surface complexation modeling in aqueous geochemistry. In: Hochella, M.F., Jr., White, A.F. (Eds.), *Mineral-Water Interface Geochemistry*, vol. 23. Mineralogical Society of America, Washington, DC, pp. 177–260.

Di Leo, P., O'Brien, P.O., 1999. Nuclear magnetic resonance (NMR) study of Cd^{2+} sorption on montmorillonite. *Clays Clay Minerals* **47**, 761–768.

Fenter, P.A., 2002. X-ray reflectivity as a probe of mineral-fluid interfaces: a user guide. In: Fenter, P.A., Rivers, M.L., Sturchio, N.C., Sutton, S.R. (Eds.), *Applications of Synchrotron Radiation in Low-temperature Geochemistry and Environmental Science*, vol. 49. Mineralogical Society of America and Geochemical Society, Washington, DC, pp. 149–220.

Fenter, P., Sturchio, N.C., 1999. Structure and growth of stearate monolayers on calcite: first results of an in situ X-ray reflectivity study. *Geochim. Cosmochim. Acta* **63**, 3145–3152.

Fenter, P., McBride, M.T., Srajer, G., Sturchio, N.C., Bosbach, D., 2001. Structure of barite (001)- and (210)-water interfaces. *J. Phys. Chem. B* **105**, 8112–8119.

Fenter, P., Teng, H., Geissbühler, P., Hanchar, J.M., Nagy, K.L., Sturchio, N.C., 2000a. Atomic-scale structure of the orthoclase (001)-water interface measured with high-resolution X-ray reflectivity. *Geochim. Cosmochim. Acta* **64**, 3663–3673.

Fenter, P., Geissbuhler, P., Dimasi, E., Srajer, G., Sorensen, L.B., Sturchio, N.C., 2000b. Surface speciation of calcite observed in situ by high-resolution X-ray reflectivity. *Geochim. Cosmochim. Acta* **64**, 1221–1228.

Fenter, P., Park, C., Cheng, L., Zhang, Z., Krekeler, M.P.S., Sturchio, N.C., 2003. Orthoclase dissolution kinetics probed by in situ X-ray reflectivity: effects of temperature, pH, and crystal orientation. *Geochim. Cosmochim. Acta* **67**, 197–211.

Ferrage, E., Tournassat, C., Rinnert, E., Charlet, L., Lanson, B., 2005. Experimental evidence for Ca-chloride ion pairs in the interlayer of montmorillonite. A XRD profile modeling approach. *Clays Clay Minerals* **53**, 348–361.

Gier, S., Johns, W.D., 2000. Heavy metal-adsorption on mica and clay minerals studied by X-ray photoelectron spectroscopy. *Appl. Clay Sci.* **16**, 289–299.

Griffoen, J., Appelo, C.A.J., 1993. Adsorption of calcium and its complexes by two sediments in calcium–hydrogen–chlorine–carbon dioxide systems. *Soil Sci. Soc. Am. J.* **57**, 716–722.

Guggenheim, S., Chang, Y.-H., Koster Van Groos, A.F., 1987. Muscovite dehydroxylation—high-temperature studies. *Am. Miner.* **72**, 537–550.

Hartman, H., Sposito, G., Yang, A., Manne, S., Gould, S.A.C., Hansma, P.C., 1990. Molecular-scale imaging of clay mineral surfaces with the atomic force microscope. *Clays Clay Minerals* **38**, 337–342.

Henderson, G.S., Vrdoljak, G.A., Eby, R.K., Wicks, F.J., Rachlin, A.L., 1994. Atomic-force microscopy studies of layer silicate minerals. *Colloid Surf. A-Physicochem. Eng. Asp.* **87**, 197–212.

Holzer, G., Wehrhan, O., Heinisch, J., Forster, E., Pikuz, T.A., Faenov, A.Y., Pikuz, S.A., Romanova, V.M., Shelkovenko, T.A., 1998. Flat and spherically bent muscovite (mica) crystals for X-ray spectroscopy. *Phys. Scr.* **57**, 301–309.

Jensen, H.E., Babcock, K.L., 1973. Cation exchange equilibria on a sandy loam. *Hilgardia* **41**, 475–487.

Karmakar, S.V., Dudley, L.M., Jurinak, J.J., James, D.W., 1991. Chloride and perchlorate influence on calcium-potassium and magnesium-potassium exchange. *Soil Sci. Soc. Am. J.* **55**, 1268–1274.

Kuwahara, Y., 1999. Muscovite surface structure imaged by fluid contact mode AFM. *Phys. Chem. Miner.* **26**, 198–205.

Kuwahara, Y., 2001. Comparison of the surface structure of the tetrahedral sheets of muscovite and phlogopite by AFM. *Phys. Chem. Miner.* **28**, 1–8.

Laudelout, H., 1987. Cation exchange equilibria in clays. In: Newman, A.C.D. (Ed.), *Chemistry of Clays and Clay Minerals*, vol. 6. Longman Scientific & Technical, Harlow, pp. 225–236.

Magnussen, O.M., Ocko, B.M., Regan, M.J., Penanen, K., Pershan, P.S., Deutsch, M., 1995. X-ray reflectivity measurements of surface layering in liquid mercury. *Phys. Rev. Lett.* **74**, 4444–4447.

Maurice, P.A., Namjesnik-Dejanovic, K., 1999. Aggregate structures of sorbed humic substances observed in aqueous solution. *Environ. Sci. Technol.* **33**, 1538–1541.

McBride, M.B., 1994. *Environmental Chemistry of Soils*. Oxford University Press, Oxford.

Namjesnik-Dejanovic, K., Maurice, P.A., 2001. Conformations and aggregate structures of sorbed natural organic matter on muscovite and hematite. *Geochim. Cosmochim. Acta* **65**, 1047–1057.

Ni, Y., Hughes, J.M., 1996. The crystal structure of nanpingite-$2M_2$, the Cs end-member of muscovite. *Am. Miner.* **81**, 105–110.

Odelius, M., Bernasconi, M., Parrinello, M., 1997. Two dimensional ice adsorbed on mica surface. *Phys. Rev. Lett.* **78**, 2855–2858.

Ohtaki, H., Radnai, T., 1993. Structure and dynamics of hydrated ions. *Chem. Rev.* **93**, 1157–1204.

Park, C., Fenter, P.A., Sturchio, N.C., Regalbuto, J.R., 2005. Probing outer-sphere adsorption of aqueous metal complexes at the oxide-water interface with resonant anomalous X-ray reflectivity. *Phys. Rev. Lett.* **94**, 076104.

Pashley, R.M., 1981. DLVO and hydration forces between mica surfaces in Li^+, Na^+, K^+ and Cs^+ electrolyte solutions: a correlation of double-layer and hydration forces with surface cation exchange properties. *J. Colloid Interface Sci.* **83**, 531–546.

Pashley, R.M., Israelachvili, J.N., 1984. DVLO and hydration forces between mica surfaces in Mg^{2+}, Ca^{2+}, Sr^{2+}, and Ba^{2+} chloride solutions. *J. Colloid Interface Sci.* **97**, 446–455.

Pashley, R.M., Quirk, J.P., 1989. Ion exchange and interparticle forces between clay surfaces. *Soil Sci. Soc. Am. J.* **53**, 1660–1667.

Pitzer, K.S., 1991. Ion interaction approach: theory and data correlation. In: Pitzer, K.S. (Ed.), *Electrolytic Solutions*. CRC Press, Boca Raton, FL, pp. 75–154.

Raouafi, S., Jeung, G.-H., Jungen, C., 1999. The electronic structure of CaCl: calculation by R matrix and generalized defect theory. *J. Mol. Spectrosc.* **196**, 248–258.

Robinson, I.K., 1986. Crystal truncation rods and surface roughness. *Phys. Rev. B* **33**, 3830–3836.

Robinson, R.A., Stokes, R.H., 1959. *Electrolyte Solutions*. Butterworths, London.

Schlegel, M.L., Manceau, A., Hazemann, J.-L., Charlet, L., 2001. Adsorption mechanisms of Zn on hectorite as a function of time, pH, and ionic strength. *Am. J. Sci.* **301**, 798–830.

Schlegel, M.L., Nagy, K.L., Fenter, P., Sturchio, N.C., 2002. Structures of quartz (10(bar1)0)- and (10(bar1)1)–water interfaces determined by X-ray reflectivity and atomic force microscopy of natural growth surfaces. *Geochim. Cosmochim. Acta* **66**, 3037–3054.

Shannon, R.D., 1976. Revised effective ionic radii and systematic studies of interatomic distances in halides and chalcogenides. *Acta Cryst. A* **32**, 751–767.

Sheldrick, G.M., 1997. *SHELXL-97, A Program for Crystal Structure Refinement*. University of Gottingen, Gottingen, Germany, Release 97-2.

Singh, U., Uehara, G., 1998. Electrochemistry of the double layer: principles and applications to soils. In: Sparks, D.L. (Ed.), *Soil Physical Chemistry*. CRC Press, New York, pp. 1–46.

Skipper, N.T., Sposito, G., Chang, F.-R.C., 1995. Monte-Carlo simulation of interlayer molecular structure in swelling clay minerals. 2. Monolayer hydrates. *Clays Clay Minerals* **43**, 294–303.

Smyth, J.R., Jacobsen, S.D., Swope, J.R., Angel, R.J., Arlt, T., Domanik, K., Holloway, J.R., 2000. Crystal structures and compressibilities of synthetic $2M_1$ and $3T$ phengite micas. *Eur. J. Mineral.* **12**, 955–963.

Sposito, G., 1984. *The Surface Chemistry of Soils*. Oxford University Press, Oxford.

Sposito, G., 1989. Surface reactions in natural aqueous colloidal systems. *Chimia* **43**, 169–176.

Sposito, G., 1991. Effect of chloride ions on sodium–calcium and sodium–magnesium exchange on montmorillonite. *Soil Sci. Soc. Am. J.* **55**, 965–967.

Sposito, G., Holtzclaw, K.M., Johnston, C.T., Levesque-Madore, C.S., 1981. The thermodynamics of sodium–copper exchange on Wyoming bentonite at 298 K. *Soil Sci. Soc. Am. J.* **45**, 1079–1084.

Sposito, G., Holtzclaw, K.M., Jouany, C., Charlet, L., 1983a. Cation selectivity in sodium–calcium, sodium–magnesium and calcium–magnesium exchange on Wyoming bentonite at 298 K. *Soil Sci. Soc. Am. J.* **47**, 917–921.

Sposito, G., Holtzclaw, K.M., Charlet, L., Jouany, C., Page, L., 1983b. Sodium-calcium and sodium–magnesium exchange on Wyoming bentonite in perchlorate and chloride background ionic media. *Soil Sci. Soc. Am. J.* **47**, 51–56.

Steele, H.M., Wright, K., Nygren, M.A., Hillier, I.H., 2000. Interactions of the (001) surface of muscovite with Cu(II), Zn(II), and Cd(II): a computer simulation study. *Geochim. Cosmochim. Acta* **64**, 257–262.

Tournassat, C., Greneche, J.M., Tisserand, D., Charlet, L., 2004. The titration of clay minerals I. Discontinuous back titration technique combined with CEC measurements. *J. Colloid Interface Sci.* **273**, 224–233.

Van der Lee, J., DeVindt, L., 1999. *CHESS Tutorial and Cookbook*. CIG-École des Mines de Paris, Fontainebleau, France.

Vrdoljiak, G.A., Henderson, G.S., Fawcett, J.J., Wicks, F., 1994. Structural relaxation of the chlorite surface imaged by the atomic force microscopy. *Am. Miner.* **79**, 107–112.

Wicks, F.J., Kjoller, K., Eby, R.K., Hawthorne, F.C., Henderson, G.S., Vrdoljak, G.A., 1993. Imaging the internal atomic-structure of layer silicates using the atomic-force microscope. *Can. Miner.* **31**, 541–550.

Wolery, T., 1992. *EQ3/6: A Software Package for Geochemical Modelling of Aqueous Systems*. Lawrence Livermore National Laboratory, Livermore, CA.

Xu, L., Salmeron, M., 1998. An XPS and scanning polarization force microscopy study of the exchange and mobility of surface ions on mica. *Langmuir* **14**, 5841–5844.